Article

Dimensioning of Reactive Power Compensation in an Autonomous Island System

Georgios N. Psarros [1,*] ⬤, **Georgios I. Tsourakis** [2] ⬤ **and Stavros A. Papathanassiou** [1]

1   School of Electrical and Computer Engineering, National Technical University of Athens (NTUA),
    9 Iroon Polytechniou Street, 15780 Athens, Greece; st@power.ece.ntua.gr
2   Independent Power Transmission Operator (IPTO) S.A., 15780 Athens, Greece; g.tsourakis@admie.gr
*   Correspondence: gpsarros@mail.ntua.gr; Tel.: +30-210-7724014

Featured Application: The proposed method has been applied in the autonomous system of Rhodes Island, Greece.

Abstract: In this paper, a method for sizing the reactive power compensation in a non-interconnected island power system is presented and applied to determine the necessary inductive reactive power compensation for the autonomous power system of Rhodes Island, Greece. The Rhodes power system is often confronted with an excess of reactive power, as a result—inter alia—of underground high-voltage (HV) cable lines and distributed generation penetration. Reactive power compensation is typically a local issue in power systems, usually aiming at maintaining an acceptable voltage profile on specific transmission segments, e.g., long underground or submarine cables. In autonomous systems, however, where network lengths are relatively short, reactive power compensation is meant to address the overall reactive power equilibrium of the system. The proposed method follows a three-step approach. First, power flow analysis is conducted to determine the size of the maximum compensation that may be necessary, i.e., the compensation size that practically allows unit commitment to be conducted without being constrained by reactive power considerations. Then, a unit commitment and economic dispatch model is executed over the course of a year to determine the optimal compensation size, using the output of the power flow analysis to formulate reactive power balance constraints. Finally, the results of the economic optimization are assessed in terms of dynamic security to verify the feasibility of the optimal solution.

1. Introduction

The autonomous power system of Rhodes Island, Greece, has recently undergone a major transformation, including the implementation of a new thermal power plant (TPP), the reinforcement and upgrade of the HV network transmission system from 66 kV to 150 kV, and the installation of a new GIS HV/MV substation fed by underground HV cable lines to supply the city of Rhodes. These developments have altered the fundamental electrical characteristics of the local power system and created challenges that had to be overcome to secure its operation. One major challenge was related to the management of excess reactive power during low demand periods, an issue typically addressed by shunt reactors, as is the case in modern power systems incorporating significant lengths of cable lines [1].

To properly size reactive compensation, voltage rise and power transfer capability limitations are taken into account in typical interconnected system planning studies [1–4]. HVAC overhead and cable lines produce substantial amounts of reactive power which may have to be transmitted over long distances, if not consumed locally, as is the case in light

load conditions. This, in turn, will impact active power transmission capability, increase losses, and give rise to significant overvoltages. VQ curves can help determine the amount of reactive compensation needed, while secondary voltage control (if applied) is in charge of shunt compensation switching, with the objective of maintaining reactive reserves on generators to face incidents [5]. Reactive compensation can significantly improve voltage stability, and the effect of its allocation and amount on the voltage stability margin is often analyzed with sensitivity analysis methods [6,7].

Traditionally, the locations for placing new VAr sources are either simply estimated or directly assumed. The optimal allocation and determination of the types and sizes of installed reactive compensation is known as reactive power planning. Recent research has presented some rigorous optimization-based methods to address reactive power planning as a security-constrained optimal power flow problem in large power systems [8–11].

In autonomous systems, excess reactive power will have to be consumed by voltage-regulating units, typically synchronous generators operating in an underexcited mode, a situation usually characterized by a reduced rotor angle stability margin and prevented by means of underexcitation limiters (UELs) [12]. However, the application of underexcitation limiters in autonomous systems should be approached with caution, as this may result in overvoltage instability, even though there may be no imminent risk of loss of synchronism [13–15]. An incident of this type occurred in Rhodes in 2016 and is analyzed in detail in [16].

As it will be further analyzed in this paper, in dealing with a small autonomous system, the main driver when sizing reactive power compensation is not voltage rise concerns in certain parts of the network, but rather the reactive power absorption capability of local generators.

An investment-oriented approach would foresee reactive power compensation facilities large enough to consume any excess VAr in the system, ensuring that reactive power issues never interfere with unit commitment and economic dispatch (UC-ED). However, such an approach would inevitably result in over-dimensioning compensation facilities. An operational approach, on the other hand, would seek a suitable unit commitment schedule, securing online units with sufficient reactive power absorption capabilities to manage excess VAr in the system. Even if a feasible UC solution does exist, such an approach would come at the detriment of operating efficiency, as reactive power constraints would impact the generation cost of the system and potentially hamper renewable energy penetration by enforcing the operation of a high number/capacity of conventional units.

The implementation of the right capacity of reactive power compensation facilities, as needed to minimize negative effects of increased reactive power absorption requirements from online generators for the autonomous power system of Rhodes, is the topic addressed in this paper. Both an investment-oriented and an operational approach are evaluated to derive the optimal size of shunt reactors needed for alleviating the reactive power equilibrium-based distortions introduced in the power system of Rhodes after reinforcement of its HV network.

To determine an acceptable commitment status of thermal units adhering to the reactive power absorption specificities of the Rhodes system, a suitable UC-ED model for islands is implemented [17,18] that has been amended to include simplified reactive power constraints. System operation is investigated under several reactive compensation levels, ranging from full to no compensation. System operation is simulated for an entire year, through consecutive execution of the daily UC-ED process. The impact of reactive power constraints on key system performance indices, such as the annual RES penetration levels, system generation cost, and operation of thermal units, is evaluated to determine the preferable size of shunt reactors from an operating cost and efficiency viewpoint. To assess the feasibility of the obtained results in terms of operational security of the system, a frequency stability analysis is performed, examining system operation at lowest annual demand and thus minimum inertia conditions. Frequency stability is assessed for two major system disturbances and three different reactive power compensation levels.

In brief, the main contribution of this study lies in the development and application of a coherent method to determine the optimum size of reactive compensators for a real-world study case island. The method quantifies the tangible system benefits deriving from the introduction of shunt reactors to a system facing VAr excess by utilizing a detailed UC-ED methodology. The proposed UC-ED model builds upon the classical MILP mathematical formulation [19–21], and further incorporates the reactive power absorption capabilities of thermal units so that they deal with the excess of reactive power generated by the HV network of the island during low load periods. The mathematical formulation incorporates reactive power equilibria during normal operating conditions, as well as events impacting the reactive power absorption capability, such as the loss of online generating units. The model employed in the paper incorporates the low-loading operation of thermal units, which has been presented in detail in a previous work of ours [22], and contributes to the feasibility of the UC solution for this specific case study. Additionally, the proposed UC-ED model complements the network analysis tools typically used for this purpose to justify a reasonable level for reactive compensation. Overall, the objective and contribution of this work is to optimally size reactive compensation in real-world island systems by concurrently evaluating several indices, including RES curtailment levels, system economics, constraints of thermal units, and operating security criteria.

The remainder of the paper is organized as follows. Section 2 describes the specificities of the Rhodes power system. Section 3 addresses how limitations in the reactive power absorption capability of synchronous generators may cause voltage instability in autonomous power systems and defines the reactive power consumption requirements of the system. Section 4 describes the mathematical formulation of the UC-ED optimization and performs the cost-benefit analysis regarding the feasibility of introducing new reactive power compensator. Section 5 presents the dynamic security assessment of the results of the cost-benefit analysis and Section 6 discusses the main conclusions. Appendix A sets out further assumptions regarding the management principles of Rhodes Island, while Abbreviations presents the notation used for the UC-ED model.

2. The Autonomous Power System of Rhodes

Figure 1 shows the 150 kV transmission network of the island of Rhodes, located in the south-eastern Aegean Sea. The non-interconnected island systems in Greece are operated by the Hellenic Electricity Distribution Network Operator, under its capacity as the non-interconnected island operator (NII-O). The principles governing the generation management in the Greek non-interconnected islands are described in [17,23].

The peak load of Rhodes exceeds 200 MW, occurring during the summer period. The lowest load periods are presented during March and November, when the total system load drops down to 35 MW. Until recently, the power generation system consisted of a single thermal power plant, the Soroni TPP, with 11 units of 207 MW total installed capacity (see Appendix A). Five wind power plants (WPPs) are also installed on the island, with a total installed capacity of 49.15 MW, while another 18.16 MW of PV units are distributed at the MV and LV levels.

As is typically the case in small autonomous power systems, frequency stability is the main challenge due to low inertia. In Rhodes, frequency stability relies on an under-frequency load shedding (UFLS) protection scheme. However, in recent years, another difficulty emerged as it became necessary for the generators of the Soroni TPP to absorb significant amounts of reactive power during low load periods, systematically requiring the underexcited operation of synchronous generators. The main reasons that led to such operating conditions are identified as follows:

- The upgrade of the transmission system from 66 kV to 150 kV, resulting in a higher reactive power generation from the HV lines.
- High MAX to MIN load ratio, which leads to a practically unloaded operation of the transmission system in low load conditions occurring in Autumn and Spring.

- Increasing number of MV cables with significantly higher capacitance compared to overhead lines.

The analysis presented in this paper demonstrates that excess reactive power generation conditions in the local system are further exacerbated by two additional developments that took place recently:

- A new TPP located in the southern part of the island entered operation, with seven units of 119 MW cumulative capacity, increasing the total length of HV overhead lines.
- A new urban HV/MV substation was installed to supply the main load center of the city of Rhodes at the north, interconnected via underground HV cable lines.
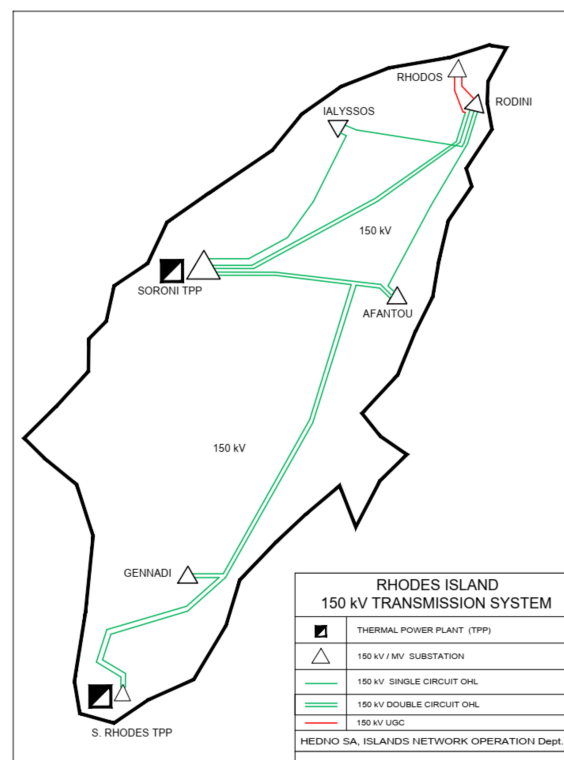

Figure 1. Rhodes 150 kV transmission network.

3. Needs for Reactive Power Compensation

3.1. Synchronous Generator Underexcited Operation in Autonomous Power Systems

For a synchronous generator to consume reactive power, it normally needs to operate underexcited. Typically, synchronous generators are protected against extensive underexcitation by (a) the UEL that will block the reduction of the excitation current below a selected threshold to prevent loss of synchronism of the generator and (b) the LOF relay that will trip the generator in case of detecting excitation loss [12]. In large, interconnected power systems, the UELs of synchronous generators play a critical role in protecting them from rotor angle instability (loss of synchronism). Additionally, the UEL is affectively set in a way to avoid the occurrence of loss-of-field incidents during normal operation.

On the other hand, the application of UELs in isolated autonomous systems should be approached with caution, given that, while there is low risk for loss of synchronism, an attempt to limit the absorption of reactive power may lead to overvoltage instability [14,15]. The diversified behavior between isolated and interconnected power systems is demonstrated by the two capacitive networks shown in Figure 2.
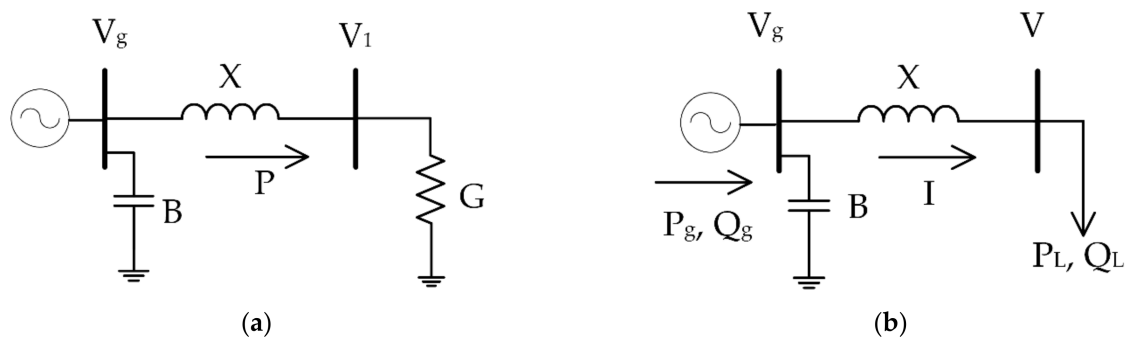
Figure 2. (**a**) One machine—infinite bus system and (**b**) autonomous power system, operating with high capacitance.

Figure 2 shows the common configuration, where an equivalent single synchronous generator is interconnected to an infinite bus through a transmission circuits represented by a series reactance X and a concentrated shunt susceptance B. With $R << X$ at the transmission level, the voltage difference between the two HV nodes of Figure 2a is approximately [24]:

$$\Delta V = V_g - V = \frac{XQ}{V} \tag{1}$$

$$Q = Q_g + BV_g^2 - XI^2 \tag{2}$$

At light load conditions, the current and reactive power losses XI^2 are low, there is significant local reactive power generation (BV_g^2), and the generator consumes reactive power ($Q_g < 0$). However, the generator reactive power absorption is limited in order to avoid decreasing the generator excitation below a predefined threshold. This function is automatically provided by the UEL of the generator. The result is the export of reactive power surplus ($Q > 0$) and a generator voltage rise ($\Delta V > 0$).

Figure 2b shows the case of an autonomous power system, where the equivalent generator feeds a small active power load. In this case, there is no way to export reactive power and the following constraint needs to be satisfied to obtain a feasible operating point:

$$Q_g + BV_g^2 = Q_L + XI^2 \tag{3}$$

Again, at light load conditions, the reactive power losses (XI^2) are low, as is the reactive power consumption of the load Q_L, which results in a very low voltage difference between the two HV nodes of Figure 2b.

Due to the above constraint (3), attempting to limit the generator reactive power absorption may result in overvoltage instability: increasing the field current increases the generator EMF and the system voltage, which results in further reactive power produced by the HV lines and consumed by the generator. Note that operating with constant excitation may also be unstable, as analyzed in [14–16]. It is therefore crucial to make use of the reactive power consumption capabilities of the synchronous generators and avoid inhibiting their automatic voltage regulation (e.g., by the underexcitation limiter or manual blocking of the excitation) to avoid voltage instability. Note also that, contrary to standard operator experience with conditions as shown in Figure 2a, the operational conditions of Figure 2b are not necessarily associated with high voltage levels. In addition, it is beneficial for the system to operate at a relatively low voltage, which is defined by the equivalent generator (and its step-up transformer, not shown in Figure 2), as this will result in lower reactive power generation.

As we analyze in detail for the case of Rhodes in Section 4, using the synchronous generators to consume excess reactive power may result in uneconomical operation, thus justifying investments in reactive power compensation.

3.2. Reactive Power Consumption Requirements in Rhodes Power System

In order to investigate whether reactive power compensation is justified, the amounts of reactive power that need to be consumed by the generators in the system of Rhodes are first calculated by means of power flow analysis. The power flow model of the transmission system shown in Figure 1 is enhanced with TPP step-up transformers, the system's HV/MV distribution transformers, equivalent models for loads and PV generation per HV/MV transformer, load compensation capacitors (out-of-service at low load conditions), and an equivalent feeder and generator for wind power plants, as shown in Figure 3.
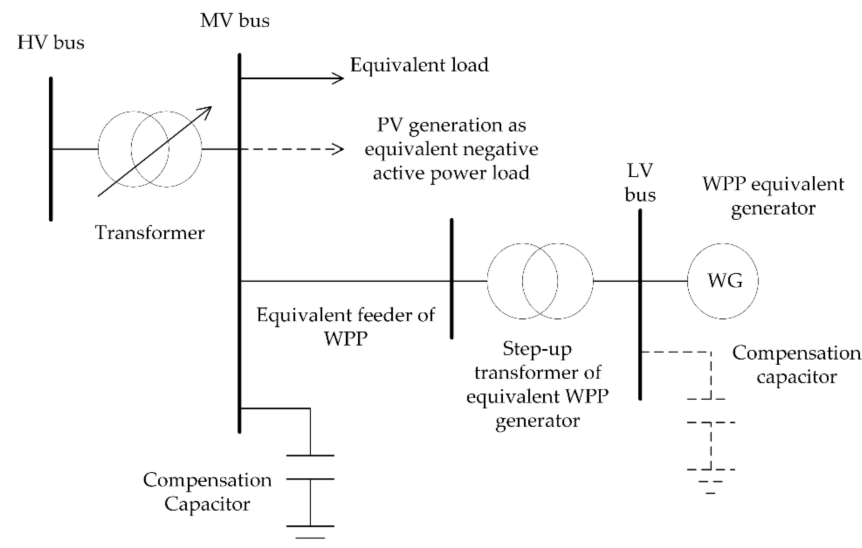
Figure 3. Model of MV network for each HV/MV distribution transformer.

The maximum reactive power consumption requirements occur under minimum load conditions (35 MW), which appear during autumn and spring nights. The equivalent load power factor is high due to a relatively extended MV cable network. Thus, a conservative assumption of unity power factor is made for the equivalent load under minimum demand conditions. WPPs are also modeled with unity p.f., as is the standard practice to minimize energy losses. Certain WPPs could consume reactive power, but the island system control center is capable of dispatching only active power setpoints. Moreover, according to available data, the installed inverters of both wind and PV power plants are not capable of operating in StatCom mode, i.e., to absorb reactive power at zero active power conditions.

HV transmission lines operate as net reactive power producers due to their significant capacitance and low loading levels. In the absence of reactive power compensation, the synchronous generators need to absorb excess reactive power, which may reach up to 27 MVAr at minimum load conditions. Excess VAr are reduced with increasing load levels, e.g., to 24 MVAr at 65 MW of demand. In the UC-ED model, the relationship between excess reactive power and system load is assumed to be linear for simplification purposes.

Due to the short distances and the autonomous nature of the local power system, sizing the reactive power compensation is not an issue of voltage drop/rise but of reactive power balance over the entire system. Therefore, the location of compensating devices does not make a significant difference in this respect, even though the installation location and the breakdown into multiple smaller compensating facilities will have to be determined with other considerations in mind, including ensuring connectivity at N-1 conditions, so that reactors remain in service in case of disturbances leading to HV circuit outages.

4. UC-ED-Oriented Cost-Benefit Analysis

To investigate the economic feasibility of introducing reactive power compensation into the power system of Rhodes, a cost-benefit analysis is performed utilizing a UC-ED

mathematical optimization model, built upon the MILP method. The model adopts a cost-optimal approach, in compliance with the generation scheduling processes applicable on the Greek islands, as described in detail in [17], suitably amended to incorporate simplified reactive power constraints for the needs of this particular system. The UC-ED optimization, performed on a 24-h horizon with a 1-hour time resolution, is consecutively executed over the course of one year. Note that the analysis is not restricted to a limited number of system operating points to determine the required size of reactive power compensators, as would be a conventional approach. Instead, it quantifies the total annual benefits in generation management that will arise out of the introduction of compensation, compared to a business-as-usual scenario of system operation without reactive compensation.

4.1. Model Fundamentals

The mathematical model for the UC-ED used in the paper is built upon the fundamentals of the MILP generation scheduling process for island systems, as described in detail in [17,18]. To enhance the flexibility of the system, the dual minimum loading technique proposed in [22] is adopted. This approach enables low load operation of the thermal units, below their normal technical minimum loading level, in a coordinated manner aiming to increase RES absorption during base-load hours without committing expensive peaking units [25–27].

The problem formulation involves constraints (4) to (20). All symbols are defined in the nomenclature section in Abbreviations. The cost minimization objective function (4) includes the variable operating costs of thermal units operating within their normal operating limits ($C_{M.I}$), the cost attributed to the low-loading operation of thermal units ($C_{M.II}$) and their start-up (C_{su}) and shut-down (C_{sd}) costs. Details regarding the definition of cost terms can be found in [17,20,22,28,29]. Equation (5) defines the active power equilibrium, while constraints (6) and (7) bound the power output of the thermal units when operating in low-load mode. Equation (8) defines the final power output of thermal units, either when in normal (over) or in low-loading (under) operation. Constraints (9) to (11) impose the commitment status of thermal units, while (12) and (13) bound their operation when in normal mode (i.e., operating within their declared minimum and maximum loading levels). Constraints (14) and (15) impose the minimum up and down times for thermal units, respectively. Constraints (16) to (18) ensure the fulfillment of reserve requirements per type (primary, secondary, and tertiary) and direction (upward/downward), while (19) limits the reserves provision per type according to the respective capabilities of each unit. Equation (20) defines the primary up reserves requirements of the system, which are crucial for island system stability during severe disturbances, e.g., the sudden loss of generation. Non-linear terms in (20) are linearized according to the methodology of [30]. For the quantification of the remaining reserves requirements, the principles of [17] apply.

$$\min\{C_{M.I} + C_{M.II} + C_{su} + C_{sd}\} \tag{4}$$

$$\sum_u P_{u,t} + (P_{w,t} - x_{w,t}) + P_{pv,t} = P_{L,t} \tag{5}$$

$$P_{u,t}^{under} \geq P_u^{rML} \cdot st_{u,t}^{under} \tag{6}$$

$$P_{u,t}^{under} \leq P_u^{TML} \cdot st_{u,t}^{under} \tag{7}$$

$$P_{u,t} = P_{u,t}^{under} + P_{u,t}^{over} \tag{8}$$

$$st_{u,t} = st_{u,t}^{under} + st_{u,t}^{over} \tag{9}$$

$$su_{u,t} + sd_{u,t} \leq 1 \tag{10}$$

$$su_{u,t} - sd_{u,t} = st_{u,t} - st_{u,t-1} \tag{11}$$

$$P_{u,t} + \sum_{r \in \{pr,sr,tr\}} r_{u,t,r}^{up} \leq P_{u,t}^{\max} \cdot st_{u,t} \tag{12}$$

$$P_{u,t}^{over} - \sum_{r \in \{pr,sr\}} r_{u,t,r}^{dn} \geq P_u^{TML} \cdot st_{u,t}^{over} \tag{13}$$

$$\sum_{k=t-T_u^{run}+1}^{t} su_{u,k} \leq st_{u,t} \tag{14}$$

$$\sum_{k=t-T_u^{stop}+1}^{t} sd_{u,k} \leq 1 - st_{u,t} \tag{15}$$

$$\sum_u r_{u,t,pr}^{up/dn} \geq rr_{t,pr}^{up/dn} \tag{16}$$

$$\sum_u \sum_{r \in \{pr,sr\}} r_{u,t,r}^{up/dn} \geq \sum_{r \in \{pr,sr\}} rr_{t,r}^{up/dn} \tag{17}$$

$$\sum_u \sum_r r_{u,t,r}^{up} \geq \sum_r rr_{t,r}^{up} \tag{18}$$

$$r_{u,t,r}^{up/dn} \leq R_{u,r} \cdot st_{u,t} \tag{19}$$

$$rr_{t,pr}^{up} = \max\left(\max_{\underaccent{\tilde}{u}}\left\{ P_{u,t} + r_{u,t,pr}^{up} \right\}, (P_{w,t} - x_{w,t}) \right) \tag{20}$$

4.2. Incorporation of Reactive Power Constraints for Thermal Units

To include the specificities of reactive power limitations on the island of Rhodes, the UC-ED is further amended by introducing relevant constraints. Note that the mathematical formulation of the UC-ED does not account for the AC power flow analysis of the system. Rather, it focuses on the reactive power absorption capabilities of thermal units, as well as the impact that the inclusion of such constraints may have on the overall UC-ED results for power systems experiencing excess reactive power during low demand periods. As analyzed in Section 3, the reactive power compensation sizing is not an issue of voltage rise, but a question of managing the reactive power absorption capability of operating synchronous generators to reasonable and secure levels.

Online thermal units should provide a cumulative reactive power absorption capability, as needed to meet the excess reactive power of the system. To ensure that the system will survive disturbances, such as the loss of generation, without compromising its reactive power absorption capability, VAr constraints should also be satisfied at G-1 conditions (loss of any online generator).

Constraints (21) to (27) ensure that online thermal units will be capable of absorbing the reactive power generated by the HV network during normal and G-1 operating conditions. More specifically, (21) forces the commitment of as many units as necessary to secure reactive absorption during normal operation (Q_t^{req} is negative when units need to absorb reactive power). Constraint (22) aims at identifying the online thermal unit that provides maximum VAr absorption capability among the committed generators. The non-linearities of (22) are properly linearized via (23) to (25). Constraint (25) identifies the generator that contributes most by setting the corresponding binary variable $z_{u,t}^Q$ equal to "1". Finally, (26) defines the status of all units after the loss of the unit that contributes the most in reactive power absorption, while (27) imposes the fulfillment of reactive power absorption requirements at G-1 operation. Note that constraint (21) is obsolete when (27) applies, yet it is included in the formulation for the sake of completeness.

$$\sum_u Q_{u,t}^{\min} \cdot st_{u,t} \leq Q_t^{req} \tag{21}$$

$$Q_t^{gen-\min} = \max_u\left\{ -Q_{u,t}^{\min} \cdot st_{u,t} \right\} \tag{22}$$

$$Q_t^{\text{gen}-\min} \geq -Q_{u,t}^{\min} \cdot st_{u,t} \tag{23}$$

$$Q_{u,t}^{\min} \cdot st_{u,t} \leq \left(1 - z_{u,t}^Q\right) \cdot M - Q_t^{\text{gen}-\min} \tag{24}$$

$$\sum_u z_{u,t}^Q = 1 \tag{25}$$

$$st_{u,t}^{rz} = st_{u,t} - z_{u,t}^Q \tag{26}$$

$$\sum_u Q_{u,t}^{\min} \cdot st_{u,t}^{rz} \leq Q_t^{req} \tag{27}$$

Similarly, constraints (28) to (34) ensure the required levels of reactive power production by online thermal units to meet demand (when the system consumes reactive power).

$$\sum_u Q_{u,t}^{\max} \cdot st_{u,t} \geq Q_t^{req} \tag{28}$$

$$Q_t^{\text{gen}-\max} = \max_u \left\{ Q_{u,t}^{\max} \cdot st_{u,t} \right\} \tag{29}$$

$$Q_t^{\text{gen}-\max} \geq Q_{u,t}^{\max} \cdot st_{u,t} \tag{30}$$

$$Q_{u,t}^{\max} \cdot st_{u,t} \geq Q_t^{\text{gen}-\max} - \left(1 - y_{u,t}^Q\right) \cdot M \tag{31}$$

$$\sum_u y_{u,t}^Q = 1 \tag{32}$$

$$st_{u,t}^{ry} = st_{u,t} - y_{u,t}^Q \tag{33}$$

$$\sum_u Q_{u,t}^{\max} \cdot st_{u,t}^{ry} \geq Q_t^{req} \tag{34}$$

Constraints (28) to (34) have been introduced within the MILP, but they do not impact the final UC-ED solution, as the reactive power production capabilities of online units far exceed the corresponding system requirements.

4.3. System Operation with and without Reactive Power Constraints

The operation of the Rhodes power system during the lowest demand day of the year is presented in Figure 4 for two cases. Figure 4a presents system operation ignoring reactive power constraints; this case effectively represents operation with a full reactive compensation scheme in place. Figure 4b refers to system operation when all reactive power constraints are introduced, without implementing any reactive compensation measures; in this case, the reactive power absorption capability of online units during the lowest demand period should exceed 27 MVAr at G-1 conditions. Figure 5 illustrates the fulfillment of system reactive power requirements by online thermal units at G and G-1 conditions for both cases described above, while Figure 6 shows the corresponding loading levels of thermal units committed to meet demand requirements.

Apparently, during the low demand intervals of the examined day (hours 00:00–08:00), where maximum reactive power absorption requirements apply, the secure operation of the system cannot be guaranteed at G-1 conditions in the absence of reactive power constraints integrated in the UC-ED (yellow solid line of Figure 5a). Note that without the introduction of reactive constraints, the operation of the system could be compromised even at G conditions, given that the four online units committed by the optimization algorithm at low demand hours (Steam#1 & ICE#7-#9) marginally fulfill the reactive power absorption requirements (red dashed line in Figure 5a). Obviously, such a UC-ED outcome would be optimal for a power system that does not face reactive power challenges, yet it cannot be acceptable for the examined case study.
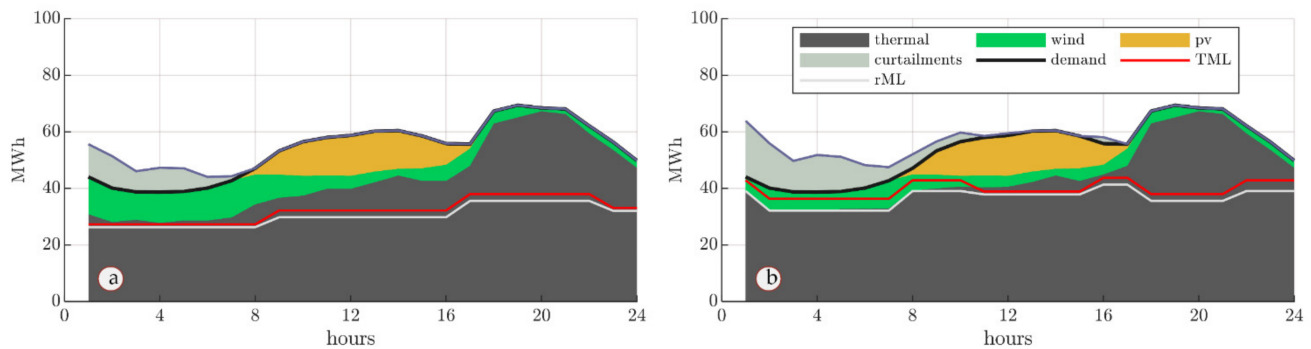
Figure 4. System operation during the lowest demand day of the year (**a**) with full and (**b**) without any reactive compensation scheme.
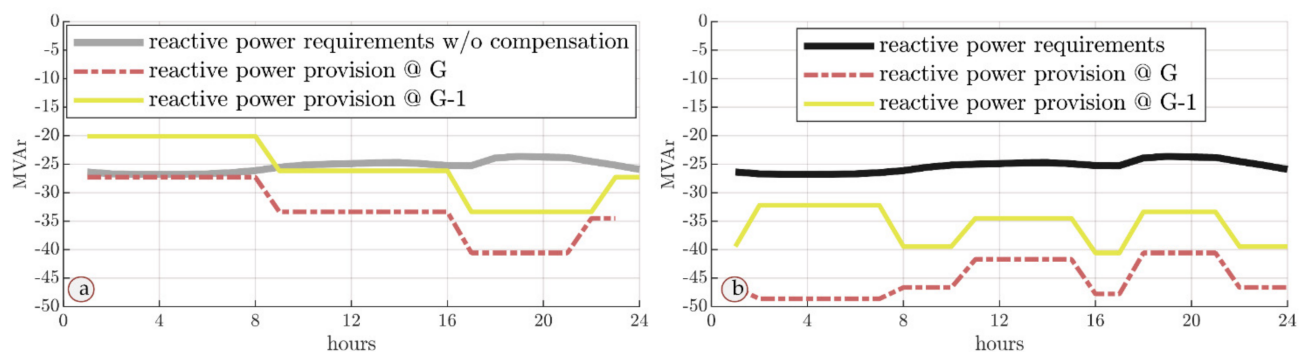

Figure 5. Fulfillment of system reactive power requirements by online thermal units at G and G-1 conditions, for the operating conditions of Figure 4.

This is circumvented by introducing constraints (21)–(27), ensuring that the committed thermal units provide the necessary level of reactive power absorption capabilities at G and G-1 conditions, as can be seen in Figure 5b. However, to achieve this, at least six generators are required to be online during the low demand hours of the examined day (Steam#1, OCGT#4, ICE#1-#2 & ICE#6-#7).

The fulfilment of system reactive power constraints comes at a cost in terms of achievable RES penetration levels, system economics, and the management of thermal units. Comparing Figure 4a,b it is apparent that RES curtailments are increased when reactive power constraints apply, due to the increased number of thermal units required to be online, which present a higher total minimum loading level (solid red line/TML of Figure 4), limiting the RES hosting capacity. This is only partially alleviated through the low load operation of thermal units during low demand periods (gray line/rML of Figure 4).

It is worth observing that the only feasible solution that concurrently fulfills the active and reactive power constraints of the problem involves the commitment of an expensive OCGT unit during the low demand hours, since the OCGT presents at the same time increased reactive power absorption capability (see Appendix A) and a very low TML, below 20% of its rated power. However, this leads to a substantial escalation in the production cost of the system, as demonstrated in Figure 7.

4.4. Reactive Compensation Requirements and Feasibility Analysis

From the analysis performed so far, it has become clear that in order to secure system operation with respect to the reactive power absorption requirements, an unreasonable unit commitment and load dispatch schedule must be applied, with an excessive number of units in operation, including peaking OCGTs during base load periods, and prolonged operation below the TML levels of the units.
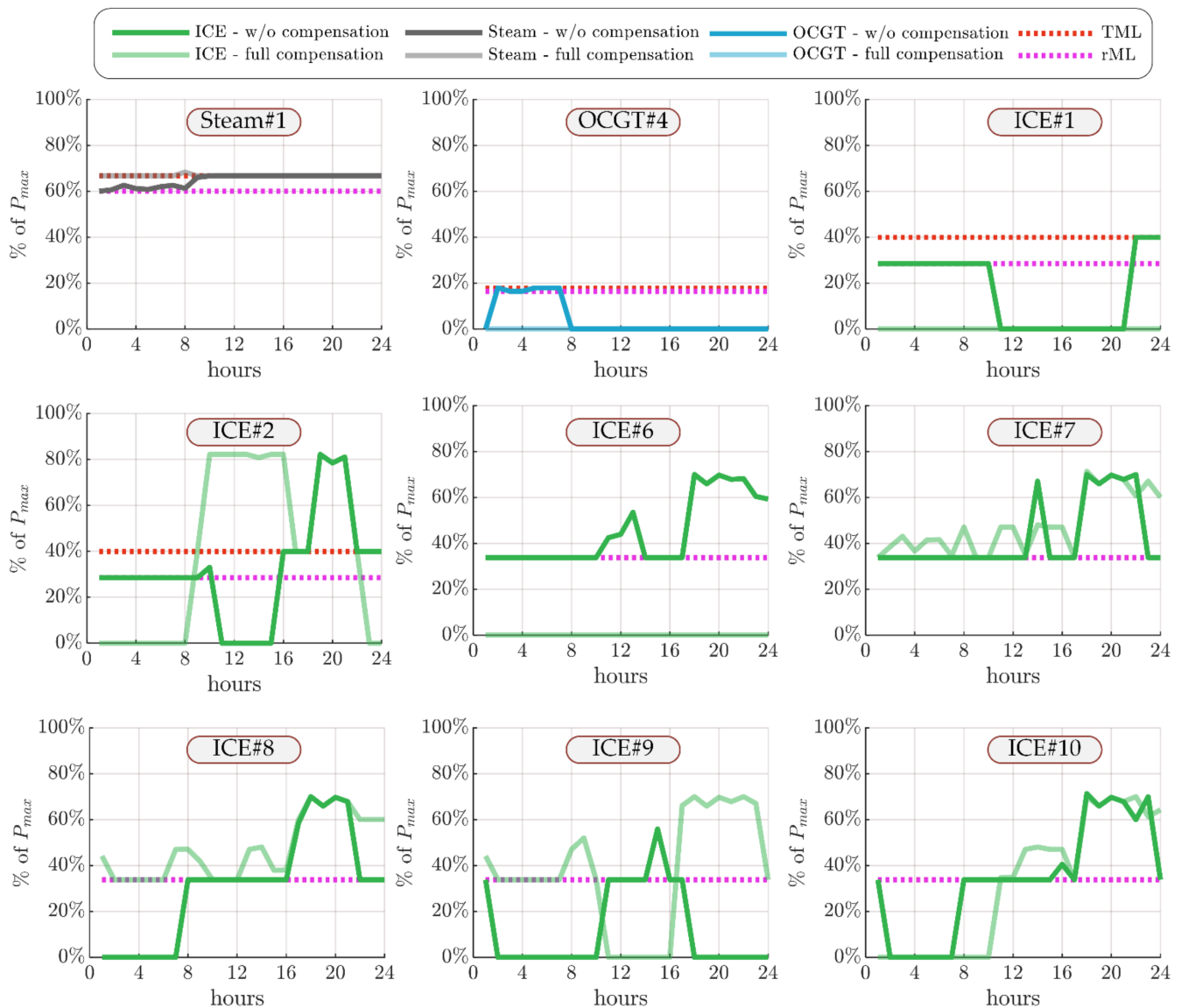
Figure 6. Loading levels of thermal units committed to meet demand requirements for the cases of Figure 4.
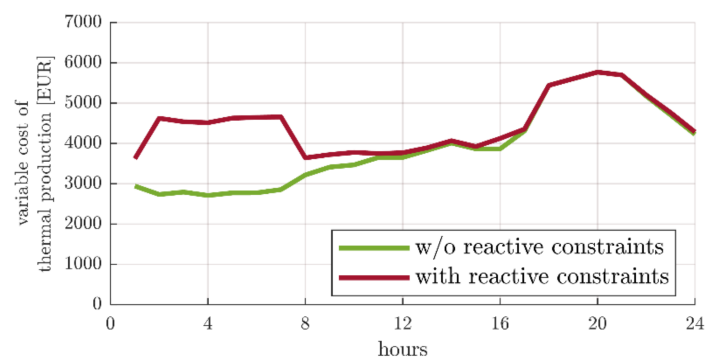

Figure 7. Hourly variable generation cost of the system in the lowest demand day, with reactive power constraints and in their absence.

To address these issues, the operation of the Rhodes power system is investigated in this section assuming seven different levels of reactive power compensation, evaluating the

positive effects on generation cost and RES curtailments, which provide the basis for the cost-benefit analysis of investments in reactive compensation. The business-as-usual/no-compensation scenario is characterized by a 27 MVAr reactive power consumption from online thermal units during low demand periods (Q^{req} = −27 MVAr). Compensating reactors are then introduced in steps of 4 MVAr capacity, as shown in Table 1.

Table 1. Examined reactive compensation levels.

Scenario	Reactive Compensation Level (MVAr, Inductive)	Q^{req} at Minimum Load
1	0	−27
2	4	−23
3	8	−19
4	12	−15
5	16	−11
6	20	−7
7	24	−3
8	27	0

Renewable curtailments and the annual duration of thermal units' operation below their technical minimum loading are presented in Figure 8 as a function of the installed reactor capacity. The introduction of appropriately sized inductive compensation can reduce both curtailments and TML violations. It appears that a reactor capacity of 12 MVAr brings about the entire anticipated benefit, reducing annual RES curtailments by 5%, from 13% to 8%, and the hours of TML violations by almost 93% (from 2400 h/y to less than 180 h/y cumulatively for all thermal units). The introduction of additional reactor capacity is pointless with regard to these performance indicators.
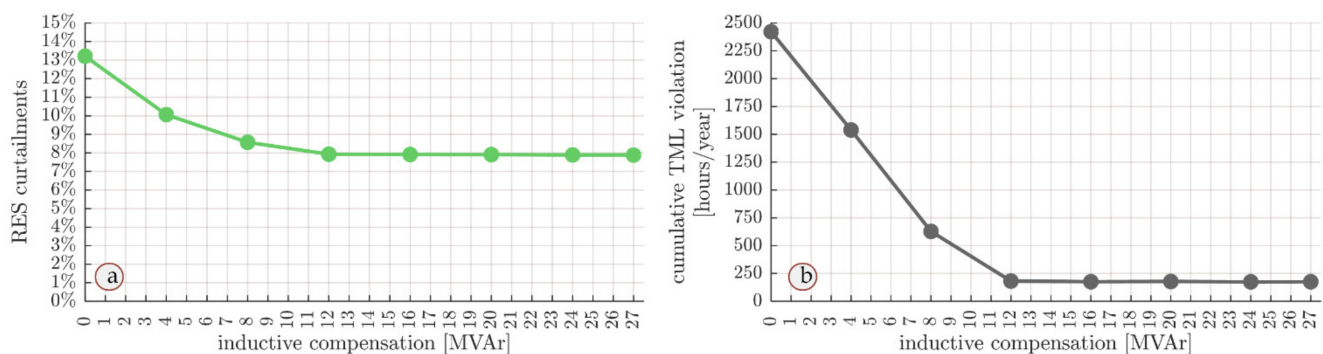

Figure 8. (**a**) RES curtailments and (**b**) annual hours of thermal unit TML violations, as a function of reactor capacity in the power system of Rhodes.

The achieved reduction in the annual generation cost of the Rhodes system through the installation of compensating reactors is shown in Figure 9. This is primarily due to two factors. First, easing reactive power constraints (21)–(27) UC-ED leads to the commitment of fewer units in low demand periods, with a lower cumulative TML and therefore more room available to accommodate renewable production. The reduction in RES curtailments shown in Figure 8 is translated into a lower system variable cost, due to the substitution of more expensive thermal generation. In addition, the commitment of expensive OCGT units during low demand periods (see Figure 6) is now avoided, resulting in further savings. Overall, significant variable cost reductions are observed for inductive compensation up to around 8 MVAr.
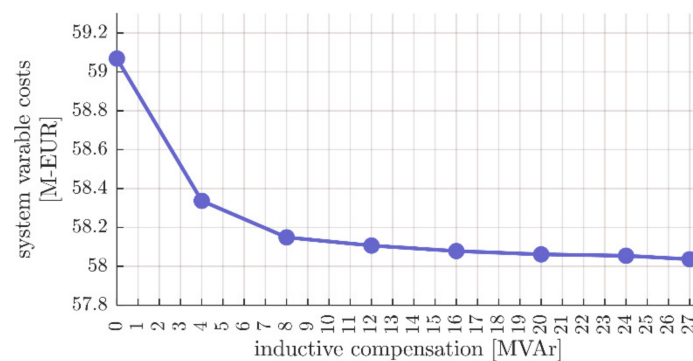
Figure 9. Reduction of system annual variable operating cost as a function of the installed reactor capacity.

The system benefit due to the presence of inductive compensation is calculated as the cost difference between the business-as-usual scenario without reactive compensation and the scenario that includes the examined size of inductive compensator.

To perform the cost-benefit analysis, the equivalent annual cost (EAC) of inductors is calculated using Equation (35), while the fundamentals of [31] apply. For the purposes of this study, the CAPEX is assumed equal to EUR 150 k/MVAr, the annual OPEX is 2% of the CAPEX, the discount rate is 5%, and the investment lifetime is assumed 15 years.

$$EAC = capex \cdot \left(\frac{d}{1 - (1+d)^{-y}} + opex \right) \tag{35}$$

The net system benefit after the implementation of reactors can be derived by subtracting the EAC of the investment from the achieved system cost savings. The results are illustrated in Figure 10, with the optimum reactor size being in the order of 8 MVAr, resulting in a net system benefit around EUR 0.8 M/year. Almost the same benefit can also be obtained with the introduction of an additional 4 MVAr of inductors (12 MVAr in total). Overall, any level of inductive compensation between 8 and 20 MVAr achieves an annual economic benefit above EUR 0.7 M.
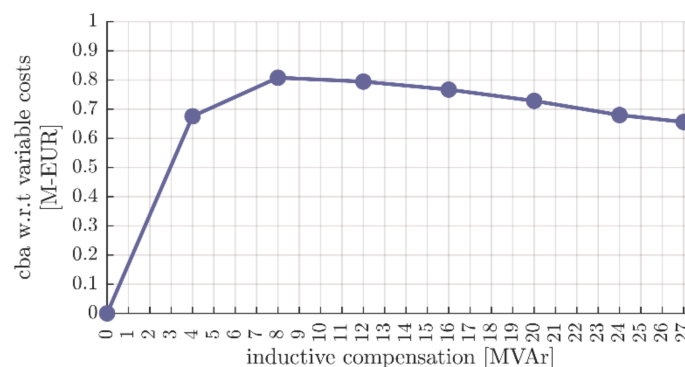

Figure 10. Cost-benefit analysis for various reactor sizes.

The sensitivity of the results to the cost of reactors is presented in Figure 11 for a CAPEX ranging between EUR 50 and 200 k/MVAr. The optimum reactor size increases as their CAPEX decreases, reaching up to 16 MVAr, with the system benefit exceeding EUR 0.9 M per year. In the increased CAPEX scenarios (EUR 150 and 200 k/MVAr), the optimum size falls to 8 MVA, with an annual gain of EUR 0.75 M in the worst-case scenario.
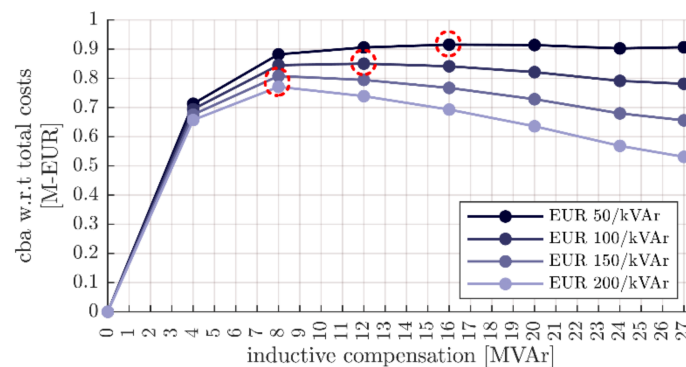
Figure 11. Sensitivity of optimal reactor size with respect to investment cost.

5. Dynamic Security Analysis

The results of the UC-ED analysis are complemented with further analysis of the system operational security. To this end, critical disturbances are simulated using a dynamic model developed in the PSS/E software that represents the particularities of the power system of Rhodes and is suitable for short-term stability analysis through fundamental frequency time domain simulations [32]. It consists of models from the PSS/E library [33] for:

- Each synchronous generator of the two TPPs with its excitation and automatic voltage regulation system, as well as its turbine and governor. The modeling parameters used are based on available manufacturer data, test measurements, and disturbance recordings. A loss of excitation distance relay model is also included.
- Dynamic models with typical parameters for each WPP modeled with one equivalent generator.
- Frequency and voltage relay models for WPPs based on the settings as set by the corresponding independent power producers.
- Frequency-dependent loads, represented in dynamic simulation as frequency-dependent admittances ($P = P_{load} \, V^2 \, \Delta f$). The reactive power load demand is assumed to be zero, per the conservative assumption of the static analysis.
- Under-frequency relay models according to the applied UFLS scheme, consisting of 13 stages, applied to 33 MV lines.

This dynamic model has been used also in the post-mortem analysis of a Rhodes blackout event [12]. Its performance has been further verified for the analysis presented herein, by comparing the simulation results of a number of events that have occurred in the Rhodes system before the S. Rhodes TPP integration to the events' available recorded data, mainly the number of MV lines shed, i.e., the number of UFLS stages activated. As an example, Figure 12 shows the response of frequency as it results from the simulation of a trip of one diesel unit generating 16 MW at low load conditions (79 MW). This resulted in the activation of four UFLS stages, tripping eight MV lines, the same as recorded. Total load shedding amounted to 6.5 MW in the simulation.

Based on the results of the UC-ED analysis, the feasibility of 4 MVAr, 8 MVAr, and 12 MVAr compensation is further examined with respect to dynamic security. In particular, minimum load conditions are examined (35 MW of system load) with the generators shown in Table 2 per case examined. RES generation is available from wind only, as minimum load conditions occur during the night.

Next, results from the analysis of two critical disturbances are presented: (a) loss a single synchronous generator after a fault (G-1 contingency) and (b) loss of the S. Rhodes TPP after a fault, resulting in the loss of its double-circuit interconnection line (N-2).

5.1. Generator Loss

The simulated disturbance consists of a three-phase fault at the HV side of the step-up transformer of the generator with the highest reactive power absorption capacity, i.e., one

of the new diesel units in S. Rhodes TPP. The fault is cleared in 100 ms with tripping of the transformer and generator. Two older WPPs (not complying with low voltage ride-through requirements) also trip in the simulation. The system is stable in all three cases, as shown in Figure 13, where the plots of voltage and frequency at the HV bus of the Soroni TPP are shown. The frequency nadir, however, ranges from approximately 49.5 Hz in the case with 4 MVAr compensation and six units in operation to less than 49.2 Hz in the case with 12 MVAr compensation and four units, as the system dynamic performance deteriorates with decreasing inertia, as expected. This results in 3.5 MW of load shed in the 12 MVAr case due to the activation of the UFLS scheme, while the latter is only marginally activated in the 8 MVAr case (1.1 MW load shed) and not activated at all in the 4 MVAr case. As a re-tuning of the UFLS is considered necessary after the latest radical system changes, no load shedding at all may be achieved also in the 8 MVAr case.
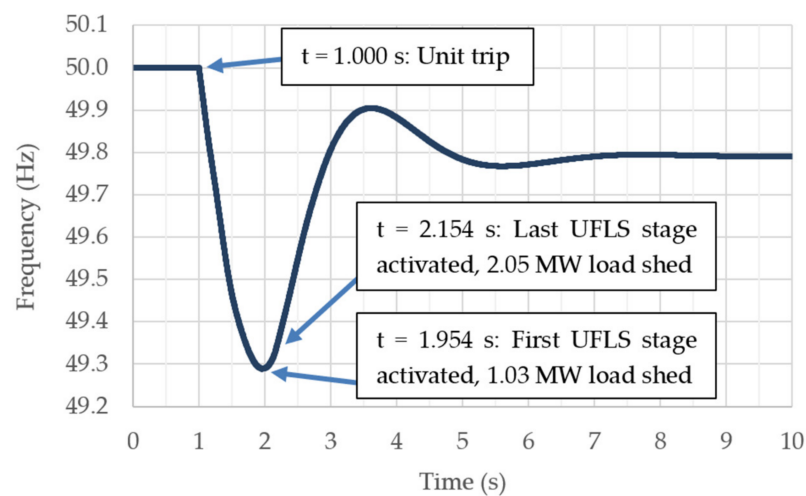

Figure 12. Simulated HV bus frequency at Soroni TPP for a single diesel unit trip.

Table 2. UC-ED results at minimum load conditions for three reactive compensation levels.

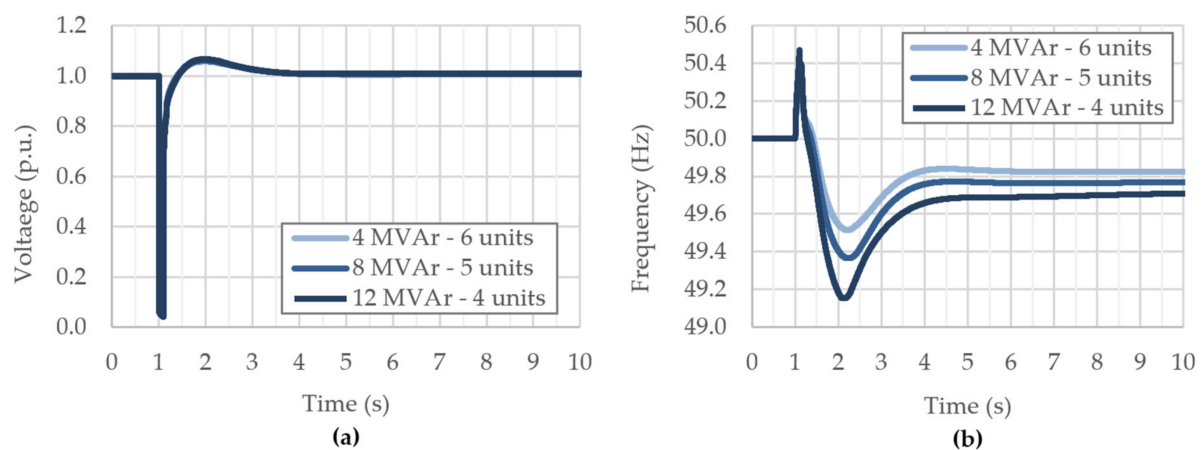| Reactive Compensation Level (MVAr, Inductive)	Thermal Units Online			Wind Power Generation (MW)
	Soroni TPP	**S. Rhodes TPP**	**Total Number of Online Units**	
4	Steam#1, ICE#1-#2	ICE#6-#8	6	5
8	Steam#1, ICE#1	ICE#6-#8	5	8
12	Steam#1	ICE#6-#8	4	12

Figure 13. HV bus voltage (**a**) and frequency (**b**) at Soroni TPP—generator trip.

5.2. Loss of S. Rhodes TPP

In the following, the critical N-2 disturbance of tripping the double-circuit OHL connecting the S. Rhodes TPP to the rest of the Rhodes transmission system following a 100 ms fault is examined. It is assumed that the compensating reactors are installed in substations Afantou and Soroni, so they remain in service after the disturbance. In such an extreme disturbance—which, however, has a significant probability of occurrence—load shedding is acceptable as a necessary means to avoid a complete blackout, which is the main concern.

Figure 14 shows the voltage and frequency at the HV bus of the Soroni TPP. Even though the voltage recovers in all cases, in the 12 MVAr case, the system is unstable as the frequency collapses. The only synchronous generator remaining in service after the disturbance is the steam turbine generator in the Soroni TPP, which is not capable of maintaining frequency stability even though extensive load shedding takes place (more than 18 MW).
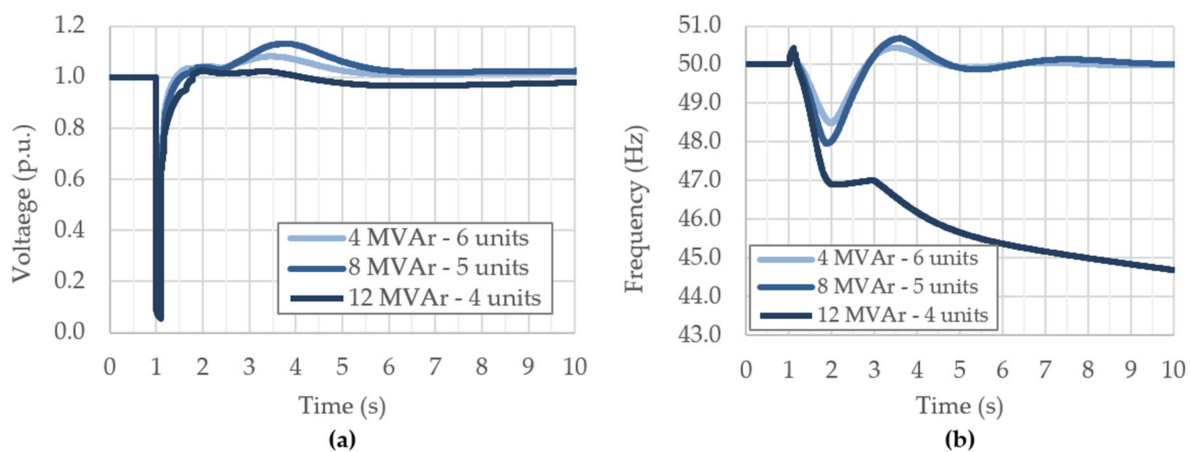

Figure 14. HV bus voltage (**a**) and frequency (**b**) at Soroni TPP—loss of S. Rhodes TPP.

6. Conclusions

This paper addresses the problem of appropriate dimensioning of the reactive compensation in the autonomous power system of Rhodes Island in Greece, which faces excessive reactive power system generation during low load periods, after major upgrades in its HV network. Against standard practice in interconnected power systems, in an autonomous system, the compensation level is not determined by local voltage management issues, but rather by the total reactive power absorption capability of voltage-regulating units, typically the synchronous generators in operation. This renders a cost-benefit analysis necessary for the problem, even though such an analysis is not typical when sizing reactive power compensation.

A comprehensive method to determine the optimum size of reactive compensators is proposed, relying on a cost-benefit analysis approach that utilizes a detailed UC-ED model to suitably quantify system benefits due to the introduction of reactors. The proposed model complements the network analysis methods typically used for this purpose.

The analysis performed in the paper indicates that the introduction of reactive power compensators in the network of Rhodes is justified from a system-level cost-benefit viewpoint. System cost estimation indicates that the introduction of 8 MVAr of reactive power compensation is optimal, while higher compensation levels (e.g., 12 MVAr) will also deliver substantial system benefits.

Simulation of system operation with and without compensation showed that reactive power compensation will have a significant impact on mitigating renewable curtailments, which can be reduced from ~13% to ~8.5% when inductors in the order of 8 MVAr are installed. RES curtailment reduction constitutes an important criterion dictating the appropriate sizing of the required reactive compensation for the network of Rhodes Island,

regardless of the system's economics, given the significance of exploiting available renewable resource towards power sector decarbonization.

Finally, dynamic security assessment revealed that attempting to harvest the economic benefits of higher compensation levels (12 MVAr and beyond) can jeopardize system security in case of critical disturbances.

Abbreviations

CAPEX	Capital expenditure
EAC	Equivalent annual cost
EMF	Electromotive force
GIS	Gas-insulated substations
HV	High voltage
HVAC	High voltage alternating current
ICE	Internal combustion engine
LOF	Loss of field
LV	Low voltage
MILP	Mixed integer linear programming
MV	Medium voltage
NII-O	Non-interconnected island operator
OCGT	Open cycle gas turbine
OHL	Overhead line
OPEX	Operating expenses
PV	Photovoltaic
RES	Renewable energy sources
rML	Reduced minimum loading
StatCom	Static synchronous compensator
TML	Technical minimum loading
TPP	Thermal power plant
UC-ED	Unit commitment and economic dispatch
UEL	Underexcitation limiter
UFLS	Under-frequency load shedding
WPP	Wind power plant

Indices

t	Index for time intervals over the optimization horizon
u	Index for conventional units
r	Index for reserve types {*pr,sr,tr,tr-ns*}, primary/secondary/tertiary spinning, and non-spinning

Binary variables

$st_{u,t}$	Binary variable equal to 1 if unit u is dispatched during period t
$st_{u,t}^{over}$	Binary variable equal to 1 if unit u is operating over its TML level during period t
$st_{u,t}^{under}$	Binary variable equal to 1 if unit u is operating between its rML and TML level during period t
$sd_{u,t}$	Binary variable equal to 1 if unit u shuts down in dispatch period t
$su_{u,t}$	Binary variable equal to 1 if unit u starts up in dispatch period t
$z_{u,t}^{Q}$	Binary variable equal to 1 if unit u contributes the most in reactive power reserves absorption in dispatch period t
$st_{u,t}^{rz}$	Binary variable equal to 1 if unit u does not contribute the most in reactive power reserves absorption in dispatch period t
$y_{u,t}^{Q}$	Binary variable equal to 1 if unit u contributes the most in reactive power reserves production in dispatch period t
$st_{u,t}^{ry}$	Binary variable equal to 1 if unit u does not contribute the most in reactive power reserves production in dispatch period t

Continuous variables

$C_{M.I}$	Actual variable generation cost of the committed thermal units over the dispatch horizon, when operating in Mode I
$C_{M.II}$	Virtual cost of the committed thermal units over the dispatch horizon, attributed to operation in Mode II
C_{sd}	Total shut down cost over the dispatch horizon
C_{su}	Total startup cost over the dispatch horizon
$P_{u,t}$	Production level of unit u in dispatch period t
$P_{u,t}^{over}$	Production level of unit u in dispatch period t for operating Mode I
$P_{u,t}^{under}$	Production level of unit u in dispatch period t for operating Mode II
$r_{u,t,r}^{up/dn}$	Reserves of type r allocated to unit u in dispatch period t
$rr_{t,pr}^{up/dn}$	Reserves requirements of type r in dispatch period t
$x_{w,t}$	Wind curtailments in dispatch period t
$x_{u,t,r}^{up/dn}$	Slack variables relaxing the reserves requirements constraints per reserve type r in dispatch period t
$Q_t^{gen-min}$	The absorbing reactive power provided by the online generator with the minimum reactive absorbing capability
$Q_t^{gen-max}$	The production reactive power provided by the online generator with the maximum reactive production capability

Parameters

$P_{L,t}$	Load demand requirements for dispatch period t
$P_{pv,t}$	Total available photovoltaic production for dispatch period t
$P_{w,t}$	Total available wind production for dispatch period t
$P_{u,t}^{max}$	Maximum power output of unit u
P_u^{TML}	Power output of unit u at TML
P_u^{rML}	Power output of unit u at rML
$R_{u,r}$	Type r reserve capability of unit u
$Q_{u,t}^{min}$	Minimum reactive absorbing capability of unit u
$Q_{u,t}^{max}$	Maximum reactive absorbing capability of unit u
Q_t^{req}	Reactive power requirements for dispatch period t
M	Big M

Appendix A

For the simulation of the power system of Rhodes, a peak load demand of 201 MW is assumed, with an annual load demand of 831.3 GWh. The thermal generation fleet includes

18 units located in two TPPs, one in Soroni and one in the southern part of the island. The main technical and economic characteristics of the thermal units are presented in Table A1.

Table A1. Technical and economic characteristics of thermal units.

TPP	Unit	S (MVA)	P^{max} (MW)	P^{TML} (MW)	P^{rML} (MW)	Q^{max} (MVAr)	Q^{min} (MVAr)	Variable Cost (EUR/MWh)
Soroni	Steam #1-#2	20.0	15	10.0	9.0	10.8	−5.7	103
Soroni	OCGT#1	26.8	20	4.0	4.0	14.4	−9.5	380
Soroni	OCGT#2	29.1	24	4.5	4.5	11.4	−3.0	326
Soroni	OCGT#3	26.3	21	5.0	4.3	14.2	−3.9	258
Soroni	OCGT#4	47.5	28	5.0	4.6	25.7	−16.4	192
Soroni	ICE#1-#2	15.4	12	4.9	3.5	8.3	−6.1	70
Soroni	ICE#3-#5	29.4	20	14.0	11.0	15.8	−8.0	81
S. Rhodes	ICE#6-#12	21.4	17	5.8	5.8	12.8	−7.2	73

To perform the cost-benefit analysis, the following assumptions have been made:

- A maximum of six daily start-ups for the Soroni and 10 daily start-ups for the S. Rhodes TPP are considered in the simulation, reflecting the current practice adopted by the NII-O for the island of Rhodes.
- Similarly, within the same dispatch period, a maximum of two simultaneous start-ups per TPP are allowed.
- For the thermal fleet of Soroni TPP, the low-loading operation mode is enabled, as proposed in [22].
- Steam unit #1 remains constantly online (must-run), as its operation is required to preheat the heavy fuel oil for the operation of ICE units in Soroni.
- Steam unit #2 remains constantly offline, effectively in cold reserve, given that the remaining conventional capacity is enough to ensure resource adequacy.

References

1. CIGRE WG C4.502. *Power System Technical Performance Issues Related to the Application of Long HVAC Cables*; CIGRE Tech. Brochure 556; CIGRE: Paris, France, 2013.
2. Glover, J.D.; Mulukutla, S.S.; Overbye, T. *Power System Analysis and Design*, 5th ed.; Cengage Learning: Boston, MI, USA, 2011; ISBN 9781111425777.
3. Lauria, S.; Gatta, F.M.; Colla, L. Shunt compensation of EHV cables and mixed overhead-cable lines. In Proceedings of the 2007 IEEE Lausanne Power Tech, Lausanne, Switzerland, 1–5 July 2007; IEEE: New York, NY, USA, 2007; pp. 1344–1349.
4. Miller, T.J.E. *Reactive Power Control in Electric Power Systems*; John Wiley & Sons: Hoboken, NJ, USA, 1982.
5. Cutsem, T.; Vournas, C. *Voltage Stability of Electric Power Systems*; Springer: Boston, MA, USA, 1998; Volume 4, ISBN 978-0-387-75535-9.
6. Begovic, M.M.; Phadke, A.G. Control of voltage stability using sensitivity analysis. *IEEE Trans. Power Syst.* **1992**, *7*, 114–123. [CrossRef]
7. Simpson-Porco, J.W.; Bullo, F. Distributed monitoring of voltage collapse sensitivity indices. *IEEE Trans. Smart Grid* **2016**, *7*, 1979–1988. [CrossRef]
8. Zhang, W.; Li, F.; Tolbert, L.M. Review of reactive power planning: Objectives, constraints, and algorithms. *IEEE Trans. Power Syst.* **2007**, *22*, 2177–2186. [CrossRef]
9. Capitanescu, F.; Martinez Ramos, J.L.; Panciatici, P.; Kirschen, D.; Marano Marcolini, A.; Platbrood, L.; Wehenkel, L. State-of-the-art, challenges, and future trends in security constrained optimal power flow. *Electr. Power Syst. Res.* **2011**, *81*, 1731–1741. [CrossRef]
10. Iba, K.; Suzuki, H.; Suzuki, K.-I.; Suzuki, K. Practical reactive power allocation/operation planning using successive linear programming. *IEEE Trans. Power Syst.* **1988**, *3*, 558–566. [CrossRef]
11. Thomas, W.R.; Dixon, A.M.; Cheng, D.T.Y.; Dunnett, R.M.; Schaff, G.; Thorp, J.D. Optimal reactive planning with security constraints. In Proceedings of the Power Industry Computer Applications Conference, Salt Lake City, UT, USA, 7–12 May 1995; IEEE: New York, NY, USA, 1995; pp. 79–84.
12. Kundur, P. *Power System Stability and Control*, 1st ed.; McGraw-Hill Education: New York, NY, USA, 1994; ISBN 978-0070359581.
13. Reimert, D. Minimum excitation limiter. In *Protective Relaying for Power Generation Systems*; CRC Press: Boca Raton, FL, USA, 2005; pp. 249–285.

14. Vournas, C.; Tagkoulis, N. Investigation of synchronous generator underexcited operation in isolated systems. In Proceedings of the 2018 XIII International Conference on Electrical Machines (ICEM), Alexandroupoli, Greece, 3–6 September 2018; IEEE: New York, NY, USA, 2018; pp. 270–276.

15. Van Cutsem, T.; Mailhot, R. Validation of a fast voltage stability analysis method on the hydro-quebec system. *IEEE Trans. Power Syst.* **1997**, *12*, 282–292. [CrossRef]

16. Vournas, C.D.; Nikolaidis, V.C.; Tsourakis, G.I. Coordinated countermeasures against overvoltage instability in autonomous power systems. *IEEE Trans. Power Deliv.* **2021**, *36*, 3329–3338. [CrossRef]

17. Psarros, G.N.; Nanou, S.I.; Papaefthymiou, S.V.; Papathanassiou, S.A. Generation scheduling in non-interconnected islands with high RES penetration. *Renew. Energy* **2018**, *115*, 338–352. [CrossRef]

18. Psarros, G.N.; Karamanou, E.G.; Papathanassiou, S.A. Feasibility analysis of centralized storage facilities in isolated grids. *IEEE Trans. Sustain. Energy* **2018**, *9*, 1822–1832. [CrossRef]

19. Ummels, B.C.; Gibescu, M.; Pelgrum, E.; Kling, W.L.; Brand, A.J. Impacts of wind power on thermal generation unit commitment and dispatch. *IEEE Trans. Energy Convers.* **2007**, *22*, 44–51. [CrossRef]

20. Carrion, M.; Arroyo, J.M. A Computationally efficient mixed-integer linear formulation for the thermal unit commitment problem. *IEEE Trans. Power Syst.* **2006**, *21*, 1371–1378. [CrossRef]

21. Psarros, G.N.; Papathanassiou, S.A. Comparative assessment of priority listing and mixed integer linear programming unit commitment methods for non-interconnected island systems. *Energies* **2019**, *12*, 657. [CrossRef]

22. Psarros, G.N.; Papathanassiou, S.A. A unit commitment method for isolated power systems employing dual minimum loading levels to enhance flexibility. *Electr. Power Syst. Res.* **2019**, *177*, 106007. [CrossRef]

23. Hatziargyriou, N.; Margaris, I.; Stavropoulou, I.; Papathanassiou, S.; Dimeas, A. Noninterconnected island systems: The Greek case. *IEEE Electrif. Mag.* **2017**, *5*, 17–27. [CrossRef]

24. Weedy, B.M.; Cory, B.J.; Jenkins, N.; Ekanayake, J.B.; Strbac, G. *Electric Power Systems*, 5th ed.; John Wiley & Sons: Hoboken, NJ, USA, 2012; ISBN 978-0-470-68268-5.

25. Chemmangot, V.N. High renewable energy penetration diesel generator systems. *Paths Sustain. Energy* **2010**. [CrossRef]

26. Hamilton, J.; Negnevitsky, M.; Wang, X. Economics of renewable energy integration and energy storage via low load diesel application. *Energies* **2018**, *11*, 1080. [CrossRef]

27. Hamilton, J.; Negnevitsky, M.; Wang, X. The role of modified diesel generation within isolated power systems. *Energy* **2022**, *240*, 122829. [CrossRef]

28. Wood, A.; Wollenberg, B.; Shebleeacute, G. *Power Generation, Operation and Control*, 3rd ed.; John Wiley & Sons: Hoboken, NJ, USA, 2013; ISBN 9780471790556.

29. Nowak, M.P.; Römisch, W. Stochastic lagrangian relaxation applied to power scheduling in a hydro-thermal system under uncertainty. *Ann. Oper. Res.* **2000**, *100*, 251–272. [CrossRef]

30. Fico MIP Formulations and Linearizations. Available online: www.fico.com (accessed on 21 December 2021).

31. European Union. *Guide to Cost-Benefit Analysis of Investment Projects*; European Commission: Brussels, Belgium, 2014.

32. Kundur, P.; Paserba, J.; Ajjarapu, V.; Andersson, G.; Bose, A.; Van Cutsem, T.; Canizares, C.; Hatziargyriou, N.; Hill, D.; Vittal, V.; et al. Definition and classification of power system stability IEEE/CIGRE joint task force on stability terms and definitions. *IEEE Trans. Power Syst.* **2004**, *19*, 1387–1401. [CrossRef]

33. Siemens PSS®E—Transmission Planning and Analysis. Available online: https://new.siemens.com/global/en/products/energy/energy-automation-and-smart-grid/pss-software/pss-e.html (accessed on 3 January 2022).